

Heterogeneous Phototransformation of Halogenated Polycyclic Aromatic Hydrocarbons: Influencing Factors, Mechanisms and Products

Yueyao Yang^{1, 2, 3}, Yahui Liu^{1, 2, 3}, Guohua Zhu², Bingcheng Lin², Shanshan Zhang^{1, 2, 3}, Xin Li^{1, 2, 3}, Fangxi Xu⁴, He Niu⁴, Rong Jin^{2, *}, Minghui Zheng^{1, 2, 3}

¹ State Key Laboratory of Environmental Chemistry and Ecotoxicology, Research Center for Environmental Sciences, Chinese Academy of Sciences, Beijing, 100085, China

² School of Environment, Hangzhou Institute for Advanced Study, University of Chinese Academy of Sciences, Hangzhou, 310024, China

³ College of Resource and Environment, University of Chinese Academy of Sciences, Beijing, 100049, China

⁴ Zhejiang Taizhou Ecological and Environmental Monitoring Center, Taizhou 318000, China

* Correspondence to: jinrong@ucas.ac.cn (R. Jin)

ABSTRACT

Chlorinated and brominated polycyclic aromatic hydrocarbons (XPAHs) are emerging pollutants widely found in atmospheric particulate matter (PM). However, their environmental transformation mechanisms remain poorly understood. In this study, we collected PM samples of varying sizes over a year for XPAH analysis and found that the average concentrations of XPAHs peaked in the winter and were dominated by the contribution of PM₁ (47.0%). Correlation analysis with relevant meteorological parameters showed strong associations between XPAH fluctuations and PM, temperatures, and humidity. Hence, controlled laboratory experiments were conducted to explore the influence of particle size, sunlight duration, temperature, humidity, and oxidant concentrations on XPAHs. Our results indicated that the transformation rates of XPAHs were influenced by the parent polycyclic aromatic hydrocarbon structures, with phenanthrene < fluoranthene < pyrene < benz[a]anthracene \approx anthracene < benzo[a]pyrene, as well as the substitution of halogens: chlorinated < brominated. Furthermore, the photo irradiation promoted the heterogeneous transformation of XPAHs; this process was accelerated by the increased concentrations of reactive oxygen species and elevated temperature, peaking at the humidity level of 45%. The transformation products were identified by nontarget analysis. According to that, we then proposed phototransformation pathways for XPAHs, suggesting a mechanism involving dehalogenation followed by oxidation. Predictions were made regarding the persistence, bioaccumulation, long-range transportation, and toxicities of XPAHs and their transformation products, showing a decrement in environmental risks as the transformation progressed. This study provides novel insights into the primary influencing factors for particulate XPAH variations and the mechanisms of heterogeneous phototransformation.

KEYWORDS: Photochemistry; Influencing factors; Heterogeneous phototransformation; Transformation mechanism; Transformation pathways;

1. Introduction

Chlorinated and brominated polycyclic aromatic hydrocarbons (ClPAHs and BrPAHs), cumulatively referred to as XPAHs, are halogenated derivatives of polycyclic aromatic hydrocarbons (PAHs) that have gained considerable attention in recent years due to their heightened persistence, toxicity, and bioaccumulation relative to their parent PAHs (Jin et al. 2017b; Ma et al. 2013; Nishimura et al. 2017; Ohura et al. 2013). At present, research on XPAHs primarily encompasses the following aspects: (1) Establishment of pre-treatment and instrumental methods (Jin et al. 2023; Liu et al. 2019b; Noro et al. 2023; Sei et al. 2021; Takikawa et al. 2023), (2) Environmental detection across various environmental media (Jin et al. 2020; Xie et al. 2021), and (3) Identification of anthropogenic sources. XPAHs have been reported to exist in the air (Jin et al. 2017c; Kakimoto et al. 2014; Nilsson and Ostman 1993), soil (Sun et al. 2013; Zhang et al. 2006), water (Shiraishi et al. 1985), sediment (Ohura et al. 2015), and organisms (Jin et al. 2017a; Liu et al. 2019b; Nishimura et al. 2017; Ohura et al. 2015; Xia et al. 2019). The sources, such as industrial thermal processes (Yang et al. 2022b), electronic waste decomposition (Wang et al. 2022), and vehicular emissions (Deng et al. 2023) have been identified, by means of detection of XPAHs in the stack gas and fly ash emitted from these sources (Jin et al. 2017b; Nishimura et al. 2017; Yang et al. 2022a). However, a significant aspect of research appears to have been overlooked: i.e. the environmental transformation. Variations in the transformation mechanisms of XPAH congeners in environmental matrices can result in differences in their environmental fate and associated risks.

The photochemical processes have been verified to represent a marked elimination pathway for organic substances affecting the atmosphere (Hu et al. 2021; Laskin et al. 2015; Malecha and Nizkorodov 2016). For example, PAHs have been confirmed to undergo oxidation (Zhu et al. 2022), or thorough fragmentation (Hu et al. 2021; Zhang et al. 2024) under atmospheric photochemical reactions. Therefore, despite the absence of direct study, given their structural similarities to PAHs, XPAHs also possess the potential to undergo similar processes. Studies by Ohura et al. also confirmed the photochemical transformation of ClPAHs when being exposed to light in cyclohexane solvent (Ohura et al. 2008). Field observations provided additional evidence suggesting that the photochemistry plays a crucial role in atmospheric XPAH transformation. For instance, certain studies have shown that concentrations of ClPAHs in particulate matter (PM) were slightly higher during nighttime than during daytime (Ma et al. 2013; Ohura et al. 2013), indicating that daytime photochemistry contributed to the

transformation of XPAHs. For BrPAHs, although no direct nighttime versus daytime concentration comparison has been conducted, prior research indicated that BrPAHs might exhibit greater instability under photo irradiation than ClPAHs (Ohura et al. 2009).

Heterogeneous reactions were identified to be the key mechanisms driving the transformation of atmospheric organic compounds, e.g., PAHs (Jia et al. 2019), during these photochemistry processes (Zhang et al. 2023). Atmospheric PM acts as a significant carrier for both environmental pollutants and catalysts, serving as a medium for heterogeneous reactions. These reactions could be influenced by various environmental factors. For instance, the reactive oxygen species (ROS) have been identified to accelerate the phototransformation of polychlorinated naphthalene (PCNs), which are two-ring ClPAHs, on the surface of silica gel (Kang et al. 2021). In addition, the temperature and humidity have been noted to influence the lifetime of atmospheric organics (Shiraiwa et al. 2011). For example, the heterogeneous oxidation mechanisms of organophosphate flame retardants were found to be significantly affected by humidity (Liu et al. 2019a). In the case of particulate XPAHs, heterogeneous reactions may also play a crucial role in their transformation. However, the influencing factors, specific mechanisms, pathways, and products remain unclear, necessitating further exploration.

This study aims to unravel the mechanisms, influencing factors, pathways, and products of XPAH heterogeneous transformation on PM. To achieve this, we conducted field studies complemented by meticulously designed laboratory experiments and nontarget organic compound analysis. Initially, we collected year-range particle samples of various sizes along with relevant meteorological data. These samples were subsequently analyzed for XPAHs. Through multivariate parameter analysis, we explored XPAH fluctuations correlated with meteorological data to pinpoint key influencing factors. Subsequently, controlled laboratory experiments were designed and conducted to unveil the heterogeneous transformation of XPAHs under the influence of particle size, humidity, temperature, and atmospheric oxidant content. The persistence, bioaccumulation, long-range transportation, and toxicities of the transformation products were then assessed to determine the environmental risks associated with XPAH transformation. Therefore, the findings of this study contribute comprehensive insights into the mechanisms and environmental risks involved in the fate of XPAHs in the environment.

2. Materials and methods

2.1 Experimental materials

In this study, a comprehensive investigation was conducted on 41 XPAHs with 2 to 5 benzene rings,

99 along with an analysis of the corresponding parent PAHs. The parent PAHs are abbreviated as follows:
100 Nap (naphthalene), Phe (phenanthrene), Ant (anthracene), Triph (triphenylene), Fluor (fluoranthene), Pyr
101 (pyrene), BaA (benz[a]anthracene), and BaP (benzo[a]pyrene). The congeners in the ClPAH and BrPAH
102 groups are described as Cl⁻, Cl₂⁻, Cl₃⁻, Cl₄⁻, Br⁻, and Br₂⁻, indicating the presence of monochlorinated,
103 dichlorinated, trichlorinated, tetrachlorinated, monobrominated, and dibrominated PAH derivatives,
104 respectively, with the numbers denoting the substituting positions. Specific names, abbreviations, and
105 molecular structures of 20 ClPAHs and 21 BrPAHs are listed in **Table S1**. As reported in our previous
106 study (Jin et al. 2017c), standards, isotopically labeled internal standards, and recovery standards for
107 XPAHs and PAHs were commercially obtained.

108 **2.2 Sample collection and extraction**

109 Atmospheric particles of three sizes (PM₁, PM_{2.5}, PM₁₀) were collected in Hangzhou from March
110 2023 to February 2024 using medium-flow samplers (Wuhan Tianhong Instruments Co., Ltd., China).
111 These samplers were positioned atop a school building at a height of approximately 15 meters above
112 ground level. The sampling site (30° 8' 15" N, 120° 4' 17" E) was situated in the Xihu District of
113 Hangzhou, with no industrial area within a five-kilometer radius. Samples were collected in monthly
114 cycles, at a flow rate of 0.1 m³/min. Quartz fiber filters were employed to capture particles. Subsequently,
115 samples were collected, dried, weighed, and stored at -18 °C.

116 Samples were extracted with a mixture of dichloromethane and hexane (1:4, v: v) by an auto-
117 Soxhlet extractor (Universal Extractor E-800, Buchi, Germany). The extracted samples were then
118 purified using an active silica column and concentrated to 50 µL using a rotary evaporator and nitrogen
119 blower. Specific processes for the extraction and clean-up processes can be found in our previous study
120 (Jin et al. 2017c).

121 **2.3 Experiments design for heterogeneous transformation of particulate XPAHs**

122 In this study, we designed a photo-transformation device that provided complete confinement and
123 precise control over the experimental conditions. The reaction unit employed a xenon lamp (light
124 intensity: 100 mW·cm⁻²) as the primary light source with an AM1.5 filter, which can achieve a good fit
125 with the sunlight spectrum, effectively simulating the outdoor solar radiation (Cao et al. 2020; Wang et
126 al. 2020). The entire photolysis reaction unit comprises a gas supply, mass flowmeters, a dryer (with
127 molecular sieve and color silica gel), a bubbler containing Milli-Q water, a xenon lamp, an optical
128 reactor, a quartz reaction vessel, a temperature control system, gas absorption bottles, and a relative

humidity monitoring component (**Fig. 1a**). To accurately emulate atmospheric conditions, model particles and a composite mixture comprising 41 XPAHs were meticulously prepared. Sequentially, 20 μL of the XPAHs mixture (1 mg/L) or individual congener solution was deposited onto the surface of the prepared layer of silica particles ($M_{\text{XPAHs}}: M_{\text{PM}} = 2\mu\text{g/g}$) (**Fig. 1b** and **Fig. S1**). The settings of the concentrations were based on previous studies on the XPAH concentrations per particle mass (Jin et al. 2017a; Jin et al. 2018). Specific information on the devices and experiments are described in **Text S1**.

To comprehensively explore the impact of various factors, including particle sizes (100 nm, 2 μm , 10 μm), temperatures (10°C, 20°C, 30°C), humidity (RH=30%, 45%, 60%), oxidant concentrations (0% (+ tert-butyl alcohol; TBA), 0%, 1%, 3%, 5%, 10%), and irradiation duration (0 min, 10 min, 30 min, 60 min, 180 min), on the phototransformation mechanism of XPAHs, a series of experiments were conducted (**Text S1**). The reacted gas was directed into a toluene solution for analysis of XPAHs in the tail gas, with less than 1% of the XPAHs escaping through volatilization during the reaction time. Dark control groups were conducted in each experiment to ensure that the difference between the two sets of experiments was due to the transformation effect caused by photo irradiation. Upon completion of the reactions, the particle layer within the reaction vessel was sonicated with 200 μL of toluene, followed by centrifugation of the supernatant. The resulting solution was then transferred into a centrifuge tube for subsequent product analysis.

2.4 Instrumental analysis

Analysis of the XPAHs and PAHs was conducted using gas chromatography coupled with magnetic sector high-resolution mass spectrometry (HRGC-HRMS, DFS, Thermo Fisher Scientific, USA) equipped with an electron ionization source. Specific information on the parameters for the oven and MS can be found in our previous study (Jin et al. 2017a). The analytical program and instrumental parameters for the analysis of PAHs were set according to “CalEPA Method 429”.

Non-target analysis of the transformation products of XPAHs was performed using a Trace 1310 GC coupled to a quadrupole-Orbitrap MS (Thermo Fisher Scientific, USA). Data were collected and processed using Thermo Scientific TraceFinder 5.1 software. High-resolution mass spectra of unknown compounds were deconvoluted into pure spectra using the Deconvolution Plugin of TraceFinder software and then verified against the standard mass spectra from the commercial library NIST 2014. Specific information on the non-target analysis was shown in **Text S2**.

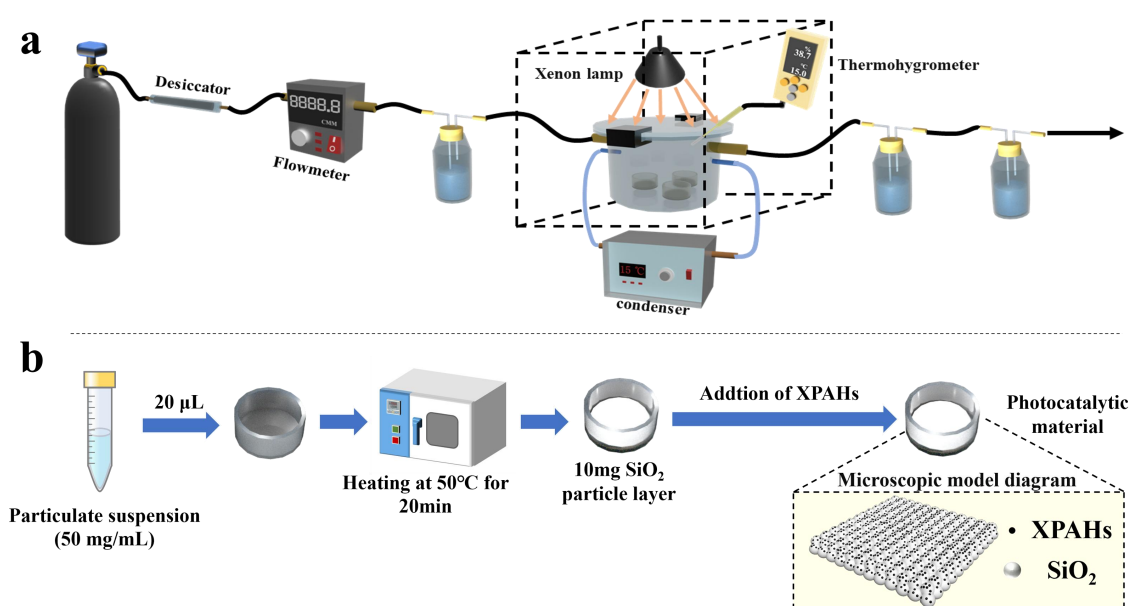
2.5 Environmental behavior and toxicity assessment of XPAHs and their transformation products

159 To assess the ecological risk and environmental characteristics—specifically, persistence, long-
 160 range transport potential, and bioaccumulation—of transformation products of XPAHs, this study
 161 employed the KOWWIN, KOAWIN, BCFBAF, and Level III fugacity models within EPI Suite 4.1 to
 162 compute various physicochemical properties of compounds. Essential environmental parameters,
 163 including molar mass, octanol-water partition coefficient (K_{ow}), air-water partition coefficient (K_{aw}),
 164 and half-lives in air, water, and soil, were subsequently introduced into the Pov-LRTP tool (Concha and
 165 Manzano 2023). Subsequently, the P-B-LRTP score is developed based on persistence (Pov),
 166 characteristic travel distance (CTD), and transfer efficiency (TE) values to prioritize the screened
 167 compounds. The respiratory toxicity model in ProTox 3.0(Banerjee et al. 2024) was used to predict the
 168 toxicity of the products, assessing their median lethal dose (LD50) and toxicity class.

$$169 \quad P - B - LRTP \text{ Score}_i = \text{LogPov} + \text{LogBAF} + \text{LogTE}$$

170 2.6 Quality assurance and quality control

171 For the analysis of actual atmospheric PM samples, the recovery rates of internal standards ranged
 172 from 52% to 105%. In laboratory simulation experiments, the recovery rates of XPAHs ranged from
 173 78% to 115%, while those of PAHs ranged from 53% to 120%. These recovery rates met the
 174 requirements for the detection and analysis of persistent organic pollutants. The detection limits (LODs)
 175 ranged from 0.17 to 1.9 fg/m³ for ClPAHs, and from 0.23 to 1.6 fg/m³ for BrPAHs. A blank sample was
 176 analyzed together with each batch of samples, and the relative concentrations of all XPAH congeners
 177 were below the detection limits.



178 **Fig. 1.** (a) The laboratory photochemical transformation setup. (b) Particulate matter preparation process.

180 3. Results and discussion

181 3.1 Occurrence levels and congener profiles of particulate XPAHs

182 During the sampling period, PM concentrations ranged from 41.5 to 653 $\mu\text{g}/\text{m}^3$, with an average
183 concentration of 130 $\mu\text{g}/\text{m}^3$ (**Fig. S2a**). PM₁ had the highest proportion, with an average of 47.0%, while
184 the proportions of PM_{1-2.5} and PM_{2.5-10} were comparable. Notably, the peak concentration was recorded
185 in April 2023. This surge coincided with a dust storm originating from the north, leading to heightened
186 levels of suspended dust in the atmosphere and a significant spike in PM levels. Barring exceptional
187 weather conditions, PM concentrations in other seasons were approximately twice as high as those
188 observed in the summer and the autumn.

189 The concentrations of $\Sigma_{21}\text{ClPAHs}$ in the particles ranged from 0.6 to 61.5 pg/m^3 (mean: 12.1
190 pg/m^3), while those of $\Sigma_{18}\text{BrPAHs}$ ranged from N.D. to 5.4 pg/m^3 (mean: 0.6 pg/m^3) during the
191 sampling period (**Fig. 2a**). These values are lower than those reported in previous studies, such as
192 Beijing, China ($\Sigma_{19}\text{ClPAHs}$: 129 pg/m^3 , $\Sigma_{19}\text{BrPAHs}$: 9.5 pg/m^3) (Jin et al. 2017a); Ulsan, South Korea
193 ($\Sigma_{11}\text{BrPAHs}$: 1.62 pg/m^3) (Vuong et al. 2020); and Shizuoka, Japan ($\Sigma_{20}\text{ClPAHs}$: 133 pg/m^3) (Ohura et
194 al. 2013). For distribution in particles of different sizes, ClPAHs had the highest fraction in PM₁ (mean:
195 45.4%, range: 29.4–65.9%) and comparable proportions in PM_{1-2.5} (mean: 28.1%, range: 13.0–52.0%)
196 and PM_{2.5-10} (mean: 26.5%, range: 8.46–3.5%). Conversely, BrPAHs showed no significant variance
197 across the three particle size ranges, with concentrations of PM₁ (mean: 35.9%, range: 12.5–68.2%),
198 PM_{1-2.5} (mean: 35.7%, range: 14.3–55.2%) and PM_{2.5-10} (mean: 28.4%, range: 1.25–59.2%) (**Fig. 2b**). In
199 total, over 70% of XPAHs were bound to particles with diameters smaller than 2.5 μm .

200 Concentration trends of XPAH homologue groups were as follows: ClFluor > ClBaP > ClAnt >
201 ClPyr > ClPhe > ClBaA (**Table S2**); BrPyr > BrPhe > BrAnt > BrTriph > BrBaA > BrFluor (N.D.)
202 (**Table S3**). The distribution profiles of XPAH congeners in PM₁₀ in Hangzhou are shown in **Fig. S2b**,
203 **Fig. S2c**, and **Table S4**. Among ClPAHs, 2-ClPhe/9-ClPhe, 1,5-Cl₂Ant/9,10-Cl₂Ant, 1-ClPyr, 3-ClFluor,
204 3,8-Cl₂Fluor, and 6-ClBaP were found to be predominant throughout the year. These distributions
205 aligned with findings of prior studies (Jin et al. 2017a; Kitazawa et al. 2006; Ma et al. 2013). It is worth
206 noting that 6-ClBaP, characterized by the highest molar mass and highest toxic equivalent factor
207 investigated within ClPAHs investigated in our study, demonstrated the highest concentration proportion.
208 BrPAHs are predominantly constituted by 2-BrPhe, 9-BrPhe, 7-BrBaA, and 1,6-Br₂Pyr. This represented
209 a notable difference from previous literature which predominantly identified 3-BrFluor, 1,8-Br₂Ant, and

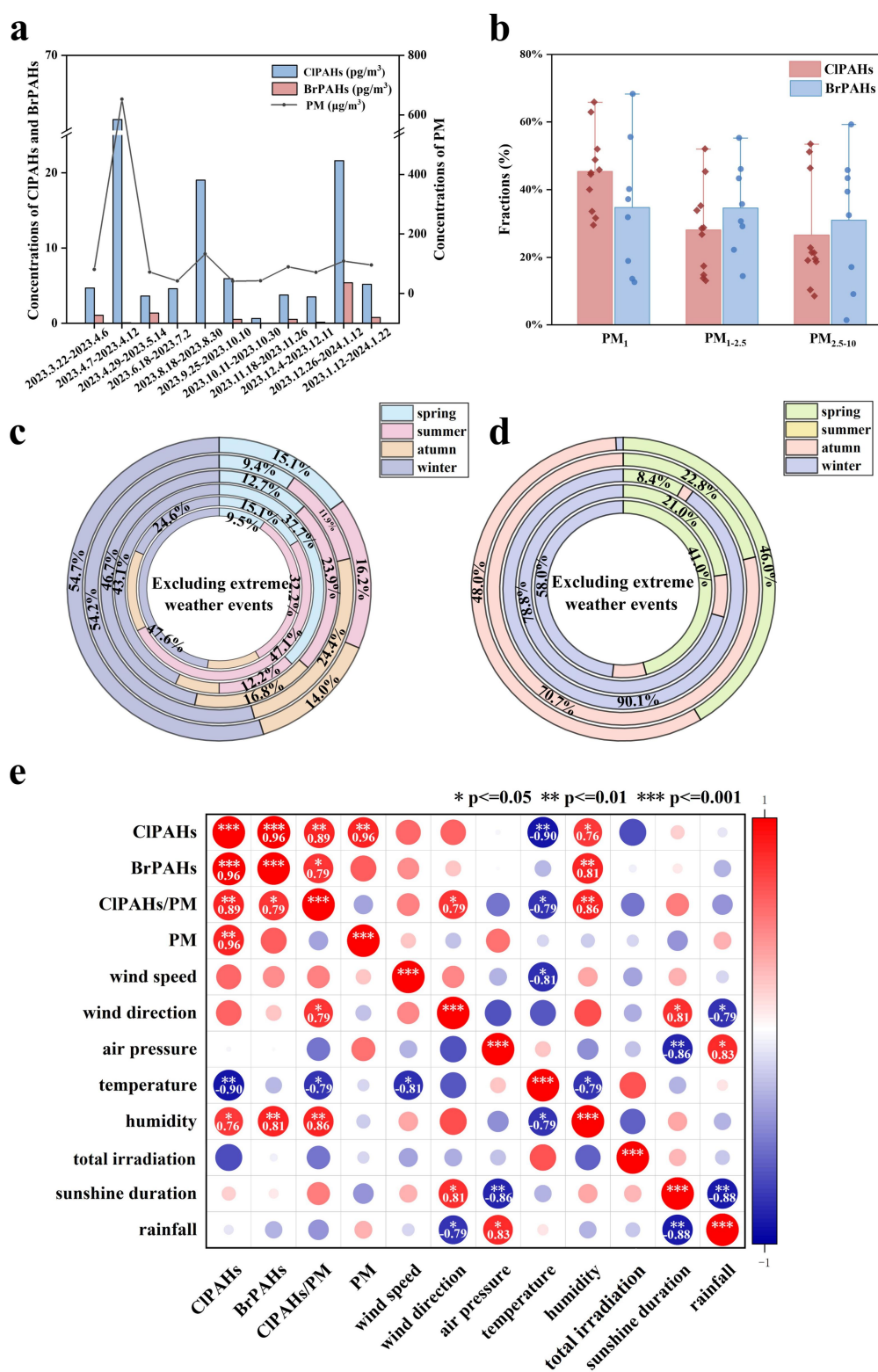
1-BrPyr as the primary congeners of BrPAHs in atmospheric PM in Beijing (Jin et al. 2017a). This disparity underscores variances in their respective sources or transformations.

3.2 Key environmental factors influencing temporal variations of particulate XPAHs

Extreme weather events such as sandstorms and prolonged light rainfall have been excluded in the following discussion. The average concentrations of PM and BrPAHs reached nadirs during the summer and the autumn while showing higher levels in the spring and the winter (**Fig. S2d**). Conversely, ClPAH concentrations remained relatively stable during the spring and the summer, decreased in the autumn, and peaked in the winter. The seasonal characteristics of ClPAHs with different parent PAH structures also varied (**Fig. 2c**). Except for ClBaA, the remaining ClPAHs reached their highest concentrations during the winter. ClFluor showed elevated concentrations in both the spring and the winter, whereas ClAnt demonstrated higher concentrations in the autumn and the winter. ClPhe maintained relatively consistent concentrations across the remaining three seasons. The seasonal characteristics of ClPAHs and BrPAHs (**Fig. 2d**) also differed. Concentrations of BrPAHs varied significantly with the seasons, with no congener detected in the summer and high concentrations of BrPhe, BrAnt, and BrPyr in the spring and the winter, likely influenced by climatic conditions such as temperature and sunshine. This disparity can be attributed to the ease of generation from sources and greater atmospheric stability of ClPAHs, while BrPAHs may be subjected to influences from atmospheric processes (Ohura et al. 2009).

Eight meteorological parameters were collected throughout the sampling period: wind speed, wind direction, air pressure, temperature, humidity, total irradiation, sunshine duration, and rainfall. Details are listed in **Table S5**, and the results of multifactor correlation analysis are shown in **Fig. 2e**. Pearson correlation analysis revealed significant positive correlations between ClPAHs and BrPAHs ($P < 0.001$, $R = 0.96$), PM ($P < 0.01$, $R = 0.96$), and humidity ($P < 0.05$, $R = 0.76$). BrPAHs exhibited a significant positive correlation with humidity ($P < 0.01$, $R = 0.81$). The impact of humidity was notably significant, as an increase in humidity tended to facilitate the upward adsorption of XPAHs onto PM. However, a previous study (Vuong et al. 2020) from Ulsan, South Korea has reported a negative correlation between humidity and XPAHs. This observation suggested that the relationship between XPAHs and humidity varied across different regions. Additionally, ClPAHs shew a significant negative correlation with temperature ($P < 0.01$, $R = -0.90$), suggesting that higher temperatures corresponded to lower ClPAH concentrations. This further elucidated the phenomenon of lower ClPAH levels observed during the summer and the autumn seasons. Other meteorological factors didn't show significant correlations with

240 CIPAHs or BrPAHs ($P > 0.05$), possibly due to the intricate interplay of multiple factors under natural
 241 conditions. Hence, the specific roles of meteorological conditions such as sunlight intensity, duration of
 242 sunshine, temperature, and humidity warranted further investigation.



243
 244 **Fig. 2.** (a) The fluctuations of concentrations of PM, Σ_{21} CIPAHs, and Σ_{19} BrPAHs in the atmosphere. (b) The
 245 proportions of CIPAHs and BrPAHs across different PM diameters. (c-d) Seasonal distributions of CIPAH (c) and

BrPAH (d) congeners, excluding events of extreme conditions, arranged from outermost to innermost layers: ClPhe, ClAnt, ClPyr, ClFluor, ClBaA, and ClBaP; BrPhe, BrAnt, BrPyr, BrTriph, and BrBaA. (e) Pearson correlation analysis between ClPAHs、BrPAHs and ClPAHs/PM with meteorological parameters (wind speed, wind direction, air pressure, temperature, humidity, total radiation, sunshine duration, and rainfall) under non-extreme weather conditions.

3.3 General transformation mechanisms of particulate XPAHs under photo irradiation

According to both preliminary research(Li et al. 2023) and the experimental results mentioned above, it is evident that meteorological conditions can significantly impact the concentrations and distributions of XPAHs on PM. Controlled laboratory experiments were conducted in this study to unveil the heterogeneous transformation mechanisms of XPAHs.

The transformation ratios of XPAHs were calculated based on the ratios of transformed XPAHs to the initial concentration $((C_0 - C_t)/C_0)$. With the increase of irradiation time, a general trend of transformation was observed across XPAH congeners (**Fig. 3**). Overall, the transformation rates of ClPAHs appeared to follow the sequence: ClPhe < ClFluor < ClPyr < ClBaA \approx ClAnt < ClBaP (**Fig. S3**). This pattern aligned with the previously reported trends in PAH photolysis rates (Phe < BaA < Ant \approx BaP) (Zhao et al. 2017), indicating strong influence by the parent PAH structures. In a combined consideration of ClPAHs and their parent PAHs, shown as “ClPAHs+PAHs” in **Fig. S3**, we also observed the formation of PAHs and decreases of total concentrations of ClPAHs and PAHs. This indicated that there were dechlorination of ClPAHs and simultaneous fragmentation of parent PAH structures during the transformation of ClPAHs.

In addition, the substitution numbers in the structures had a strong influence on the transformation of ClPAHs: with increment of the substitution numbers, the transformation ratios progressively decreased (**Fig. 3**). For example, after 1 h of irradiation, transformation ratios were approximately 20% for 3-ClPhe and 2-ClPhe/9-ClPhe, while 10% for 9,10-Cl₂Phe. An exception was observed for ClAnt congeners (1,4-Cl₂Ant or 1,5-Cl₂Ant/9,10-Cl₂Ant < 1-ClAnt/2-ClAnt or 9-ClAnt < 1,5,9,10-Cl₄Ant. This difference could be attributed to the fact that the investigated low-chlorinated ClAnts are dechlorination products of high-chlorinated ClAnts. While the substitution position had some impact, it was not as significant as the number of chlorines. For instance, both 2,5-Cl₂Fluor and 3,8-Cl₂Fluor demonstrate comparable photolysis extents, with approximately 20% transformation after 30 min of irradiation, and transformation ratios of 68.8% and 49.4% after 3 h of irradiation, respectively.

For BrPAHs (**Fig. S4**), the overall transformation ratio ranked as follows: BrPhe < BrAnt < BrPyr \approx BrFluor < BrBaA < BrBaP. The transformation ratio ranking between BrPAHs and ClPAHs exhibited disparities, implying that distinct halogen substitutions might yield diverse transformation effects. BrPAHs degraded more rapidly than ClPAHs. For example, BrPyr degraded by 60% after 30 min of irradiation, while ClPyr only degraded by less than 40%. Additionally, the increase in degree of bromination didn't appear to have a notable effect on the transformation rate of BrPAHs, which differed from ClPAHs.

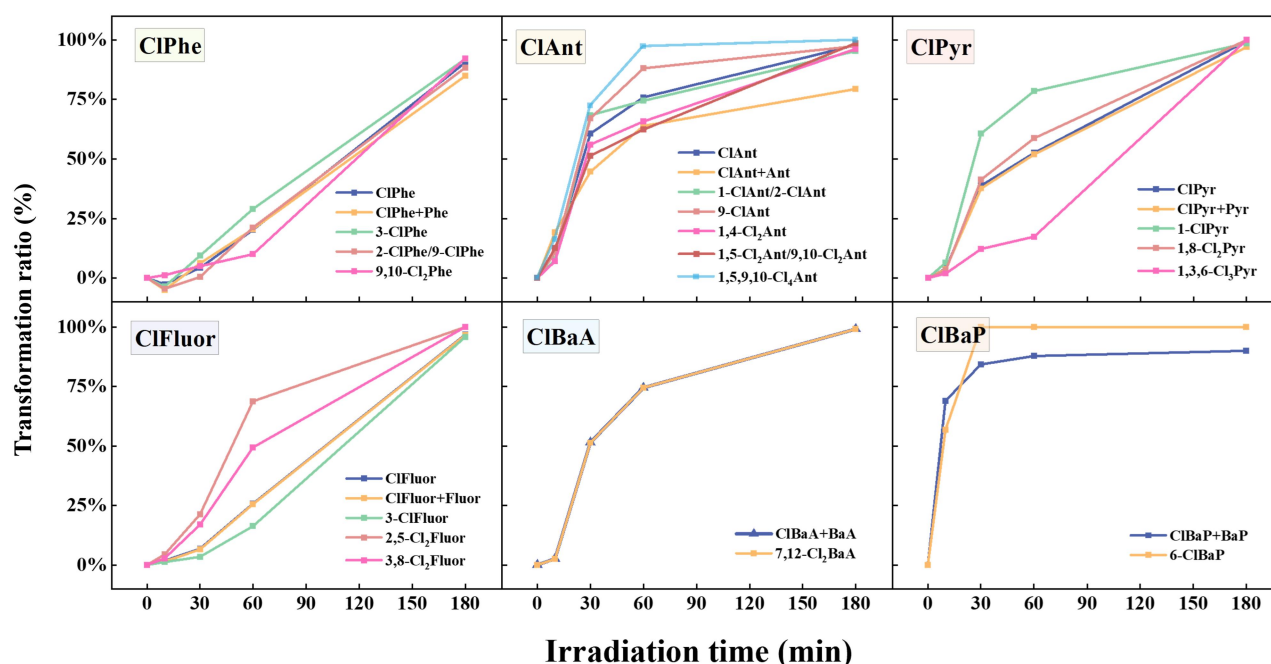


Fig. 3. The relationships between transformation ratios of ClPAHs and photo irradiation time.

3.4 Influencing factors for heterogeneous transformation of particulate XPAHs

The influencing factors, i.e., particle size, relative humidity, reactive oxygen species content, and temperature on XPAH transformation have been investigated (**Text S1**). Although previous studies have revealed variations in XPAH concentrations on particles of different sizes (Jin et al. 2017a; Lara et al. 2022; Ma et al. 2013), the influence of particle size (100 nm, 2 μ m, and 10 μ m) on transformation efficiency was found to be not notably significant in simulated experiments (**Fig. S5 and Text S3**).

The influence of humidity varied among ClPAHs with different parent structures (**Fig. 4a**). For instance, the transformation of ClPhe and ClFluor slowed down with increasing humidity, whereas the transformation of ClAnt, ClPyr, ClBaA, and ClBaP increased with higher humidity levels, with the highest transformation ratio observed at 45% humidity. Additionally, we found that the impact of

humidity on transformation was not consistent for ClPAH congeners in the same homologue groups. For example, transformation of 9,10-Cl₂Phe decreased more sharply than the other ClPhe congeners with the increment of humidity. The combined influence of photo irradiation and humidity enhanced the transformation of individual ClPAHs (**Fig. S6**). For example, under 45% humidity, ClPyr exhibited an average transformation of 50% in darkness, while this rate increased to 75% under photo irradiation. Possible reasons could be that the addition of photo irradiation drove the formation of hydroxyl radical ($\cdot\text{OH}$), which could participate in the breakdown of molecules (Zhang et al. 2023). In contrast, the acceleration of transformation with increasing humidity was relatively universal for BrPAHs, with the most significant effects observed within the 30-45% humidity range (**Fig. S6c** and **Fig. S6d**).

Transformation ratios of XPAHs increased as temperatures rose, with the most significant transformation observed at 30 °C (**Fig. 4b**), indicating that the elevated temperature promote the transformation of XPAHs. The transformation ratio of each congener gradually increased with temperature compared to dark conditions (**Fig. S7a**). Under photo irradiation at the same temperature, the transformation ratios of nearly all XPAH congeners increased by more than 50% compared to dark conditions. This indicated that the breakdown of XPAH molecules was enhanced by the photo irradiation. In both photo irradiation and dark conditions, the transformation ratios of BrPAHs (**Fig. S7c** and **Fig. S7d**) exceeded those of ClPAHs. This phenomenon can be attributed to the differences in bond strength (the bond energy of C-Br is lower at 291 kJ/mol, whereas the bond energy of C-Cl is 345 kJ/mol) (Ohura et al. 2009) and atomic size (the radius of the Cl atom is approximately 99 pm, while the radius of the Br atom is around 114 pm) (Shannon 1976).

Adding H₂O₂ to the reaction system simulates the effects of oxidants present in the atmosphere on the impact of XPAH transformation under photochemical conditions. The transformation of ClPAHs accelerated with the increase of H₂O₂ concentration (**Fig. 4c** and **Fig. S8**). TBA was introduced to eliminate the $\cdot\text{OH}$ effect in the control group. Under 1-hour photo irradiation conditions, the transformation rate ranking of ClPAHs is as follows: ClBaP > ClBaA > ClPyr > ClPhe > ClAnt > ClFluor. The transformation of ClFluor showed no significant change with H₂O₂ content, indicating relative stability. Additionally, compared to monochlorinated compounds, the overall transformation ratios of polychlorinated compounds are relatively slower and less influenced by H₂O₂ (except for 1,5,9,10-Cl₄Ant). This also suggested that the dechlorination process was more pronounced in high-chlorinated compounds, while the transformation of low-chlorinated substances was mainly due to ring-

opening reactions. The situation was similar for BrPAHs, with transformation rates faster than those of CIPAHs.

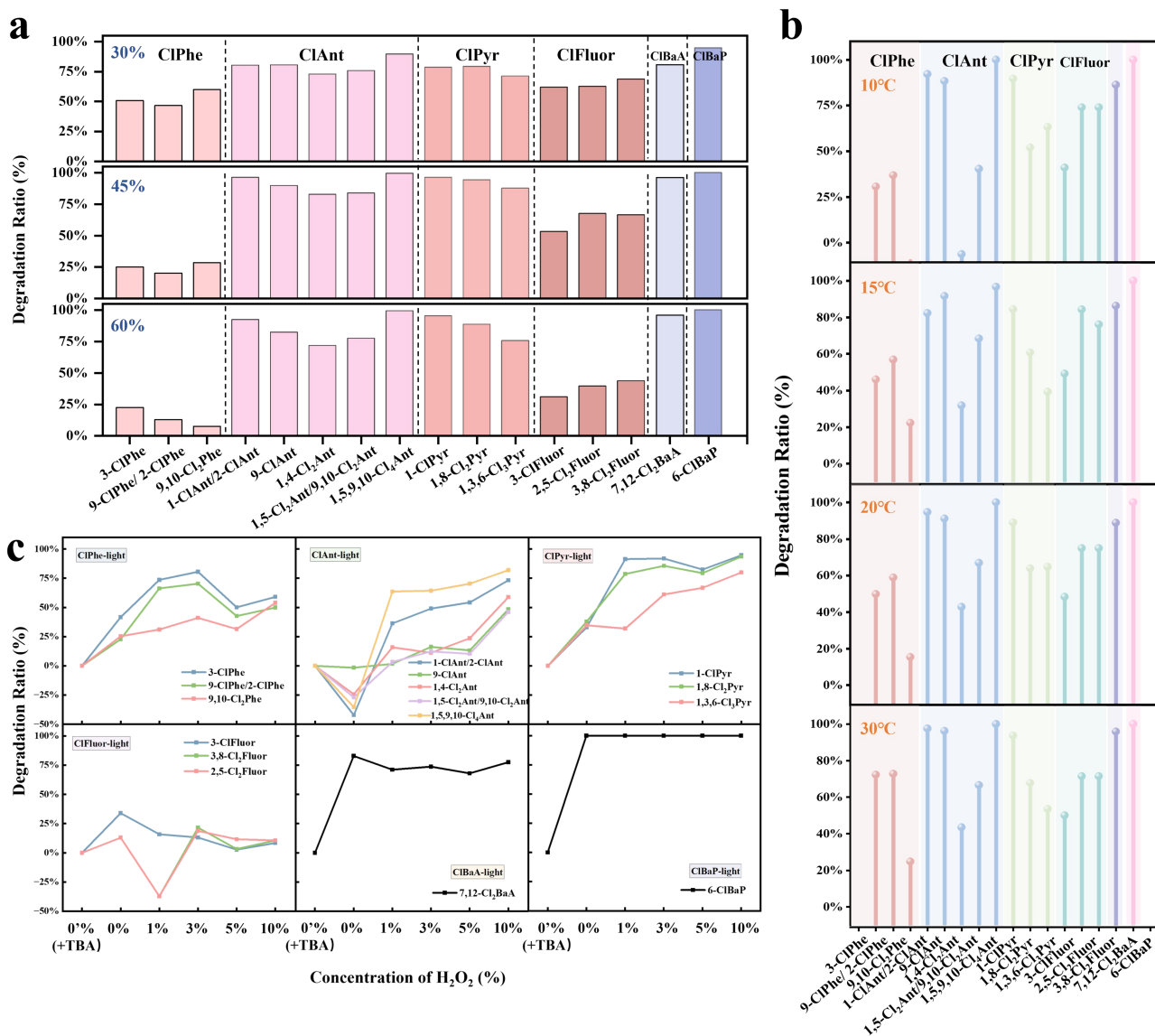


Fig. 4. Transformation ratios of CIPAHs under varying (a) humidity levels, (b) temperature conditions and (c) H₂O₂ concentrations, with photo irradiation.

3.5 Heterogeneous transformation pathways of XPAHs under photo irradiation

According to the results above, there are dechlorination, direct ring-opening, or ring-opening induced by oxidation processes involved in the breakdown of XPAHs. To elucidate the specific transformation pathways of XPAHs, we conducted photolysis experiments on highly chlorinated XPAHs, including 1,4-Cl₂Ant, 9,10-Cl₂Phe, 1,8-Cl₂Pyr, 2,5-Cl₂Fluor, 7,12-Cl₂BaA, and 6-ClBaP, individually. Non-target analysis was then employed to recognize the transformation products of these congeners.

Specific mass spectrums can be found in **Fig. S9**, and the relative compounds are listed in **Table S6**. The predominant products were quinones, ketones, hydroxyl-bearing compounds, and ring-opened products, consistent with previous findings on PAH phototransformation products (Jia et al. 2019; Zhao et al. 2017). Surprisingly, no chlorinated oxides were detected. Further analysis of the products from experiments on both ClPAHs and BrPAHs revealed no significant differences. As a result, we confirmed a hypothesis proposed in previous studies (Ohura et al. 2009) that the transformation of XPAHs underwent dehalogenation to form PAHs before oxidation.

The transformation pathways are presented in **Fig. 5**. According to the non-target analysis results of the photolysis products, the primary products for most ClPAHs, with the exception of ClFluor, were the parent PAHs in the initial step. And for ClFluor, the initial step involved not only the dechlorination, but also ring-opening, resulting in the generation of 2,7-dichlorofluorene and 9-chlorofluorene. Research findings suggested that in the atmosphere, the primary reactions for the destruction of aromatic compounds were the addition or substitution with $\cdot\text{OH}$ (Dang et al. 2014). At the same time, the substitution of H or Cl in the main structures of ClPAHs or PAHs by the $\cdot\text{OH}$ could influence the products of the next steps. Therefore, the subsequent steps might include ring opening, oxidation, or hydrolysis.

Specifically, there were three potential pathways for the transformation of 1,4-Cl₂Ant (**Fig. 5a** and **Fig. S9a**). In the first pathway, 1,4-Cl₂Ant could undergo substitution by $\cdot\text{OH}$ to form A2 (1,4-dihydroxyanthracene, C₁₄H₁₀O₂), which further oxidized to produce A3 (1,4-anthraquinone, C₁₄H₈O₂). For the second and third pathways, 1,4-Cl₂Ant underwent dechlorination to yield A1 (Ant, C₁₄H₁₀). The subsequent steps were then similar to those of Ant, with oxidation leading to the formation of A4 (9,10-Anthracenediol, C₁₄H₁₀O₂), and further oxidation to A5 (9,10-Anthraquinone, C₁₄H₈O₂) as the second pathway. In the third pathway, ring-opening occurred to form A6 (2-Methylnaphthalene, C₁₁H₁₀), followed by subsequent chain-breaking ring-opening to form A7 (Nap, C₁₀H₈), A8 (1,2,3,4-Tetrahydronaphthalene, C₁₀H₁₂), and A9 (2-Methoxyphenol, C₇H₈O₂), ultimately yielding A10 (3-Nonanol, C₉H₂₀O) and A11 (3-Nonanone, C₉H₁₈O). Similar transformation pathways were observed for 9,10-Cl₂Phe (**Fig. 5b** and **Fig. S9b**), 1,8-Cl₂Pyr (**Fig. 5c** and **Fig. S9c**), and 7,12-Cl₂BaA (**Fig. 5e** and **Fig. S9e**), involving dechlorination to generate PAHs, followed by attack by $\cdot\text{OH}$ to produce phenols, further oxidizing to form quinones, acids, and esters. Additionally, 9,10-Cl₂Phe exhibited an additional oxidation pathway involving ring-opening oxidation, yielding B9 (9-Fluorenone, C₁₃H₈O), followed by a

series of chain-breaking ring-opening reactions to sequentially generate B10 (Benzophenone, C₁₃H₁₀O), B11 (3'-Methylacetophenone, C₉H₁₀O), and B12 (3-Nonanone, C₉H₁₈O). 1,8-Cl₂Pyr also had two additional potential transformation pathways. In the first pathway, uniform cleavage occurred both above and below the pyrene molecule, generating C4 (Nap, C₁₀H₈) and C5 (2-Methylnaphthalene, C₁₁H₁₀). In the second pathway, diagonal cleavage resulted in the identification of two products: C6 (2-(2,5-dimethylphenyl)-1,4-dimethylbenzene, C₁₄H₁₄) and C7 (4,4'-Dimethyldiphenyl, C₁₄H₁₄). C6 underwent attack by ·OH/O₂⁻ radicals to ultimately form C8 (Benzophenone, C₁₃H₁₀O), followed by further ring-opening cleavage to produce C9 (3'-Methylacetophenone, C₉H₁₀O). Similarly, C10 (2-Phenylpropionaldehyde, C₉H₁₀O) was formed by oxidation-induced chain-breaking of C8.

For ClFluor (**Fig. 5d** and **Fig. S9d**), the initial step involved ring-opening, generating D1 (2,7-Cl₂Fle, C₁₃H₈Cl₂) and D2 (9-ClFle, C₁₃H₉Cl). Subsequent dechlorination and ring-opening led to the formation of D3 (4,4'-Dimethyldiphenyl, C₁₄H₁₄), D4 (2-(2,5-dimethylphenyl)-1,4-dimethylbenzene, C₁₄H₁₄), and D5 (Benzophenone, C₁₃H₁₀O) in the samples. In the second pathway, the initial dechlorination process resulted in the formation of D6 (Fluor, C₁₆H₁₀), which yielded D7 (1H-Indene, 2,3-dihydro-4,7-dimethyl-, C₁₁H₁₄) and D9 (Nap, C₁₀H₈). D7 underwent bond cleavage to form D8 (1H-Indene, octahydro-, C₉H₁₆), while D10 (1,2-Diethylbenzene, C₁₀H₁₄) was the ring-opening product of D9. Further oxidation (alcohol to aldehyde) sequentially yielded D11 (1,2-Dicarboxybenzene, C₈H₆O₄) and D12 (Dibutyl phthalate, C₁₆H₂₂O₄).

6-ClBaP, as a mono-chlorinated compound (**Fig. 5f** and **Fig. S9f**), exhibited the highest phototransformation ratio among all ClPAH congeners. After dechlorination, the initial step generated F1 (BaP, C₂₀H₁₂). Among them, positions 3, 6, and 12 of BaP were particularly reactive, and ·OH attacks led to the formation of F2, F3, and F4 (6-Benzo[a]pyrenol, 6,12-Dihydroxybenzo[a]pyrene, and 9,12-Dihydroxybenzo[a]pyrene, C₂₀H₁₂O), subsequently further generated F5, F6 and F7 (6-Benz[a]pyrenone, Benzo[a]pyrene-6,12-dione, and Benzo[a]pyrene-3,6-dione, C₂₀H₁₀O₂). Under light exposure, F6 underwent further oxidation and ring-opening to produce F8 (Lapachol, C₁₅H₁₄O₃), F9 (2,6-Diisopropylnaphthalene, C₁₆H₂₀), and F11 (Dimethyl phthalate, C₁₆H₂₂O₄), as reported by S. Zhao et al (Zhang et al. 2023). The exploration of XPAH transformation is limited by the absence of quantification of the products. Further studies are necessary to elucidate the specific molecular assignments.

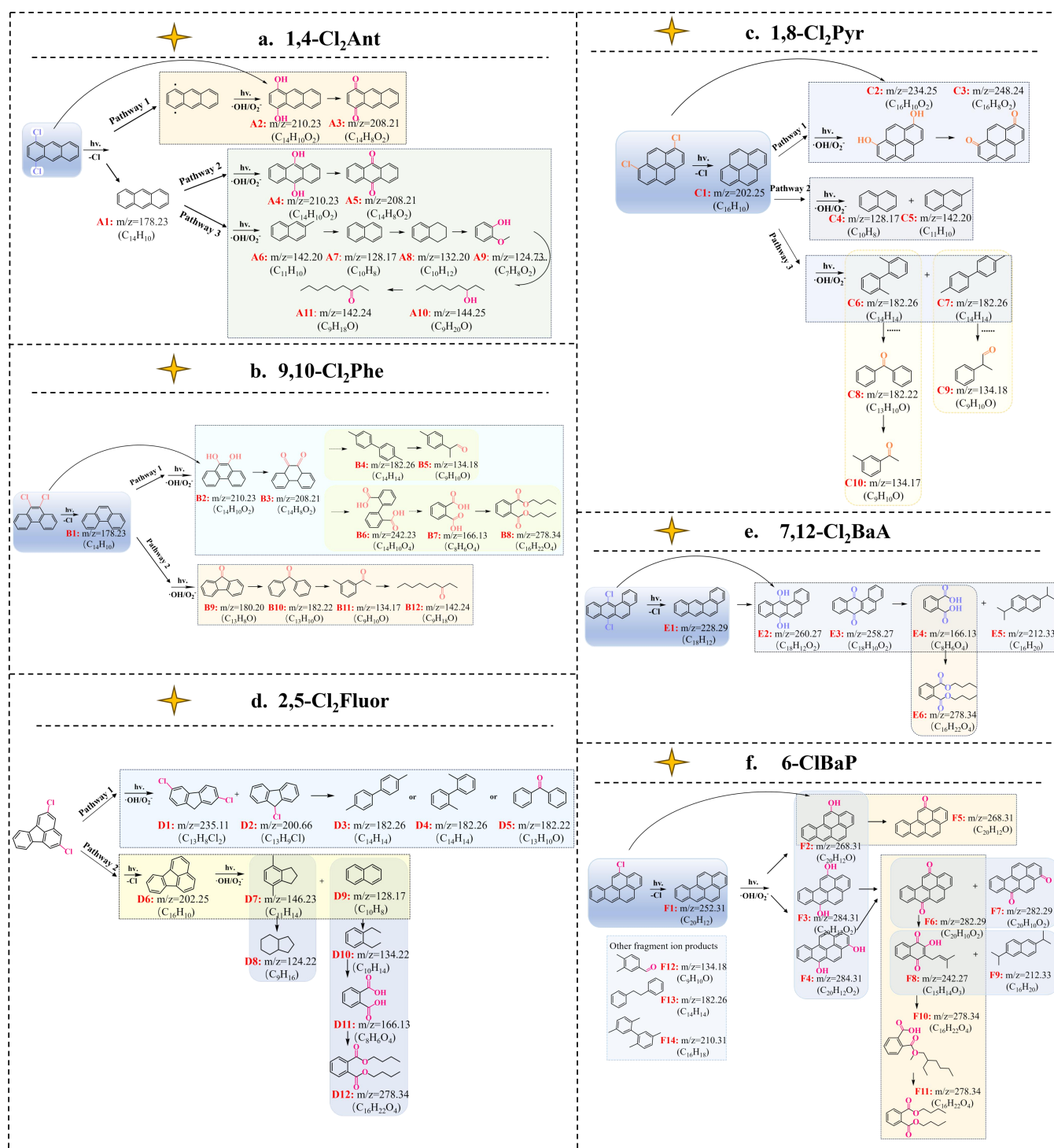


Fig. 5. (a-f) The transformation pathways and relative products of CIPAHs. ((a) 1,4-Cl₂Ant; (b) 9,10-Cl₂Phe; (c) 1,8-Cl₂Pyr; (d) 2,5-Cl₂Fluor; (e) 7,12-Cl₂BaA; (f) 6-ClBaP).

3.6 Assessments of persistence, bioaccumulation, long-range transportation and toxicities of XPAHs and their transformation products

Studies have suggested that transformation products of organic pollutants might exhibit distinct environmental behaviors and heightened ecological toxicity (Zhang et al. 2023). For the assessed P-B-

LRTP scores of XPAHs and their transformation products in this study (**Fig. 6a** and **Table S6**), it could be observed that as the transformation pathways progressed, the scores of the transformation products decreased. For instance, the score of 9,10-Cl₂Phe was 5.07, which decreased to 2.13 after dechlorination, and further oxidation products have even lower scores ranging from 1.65 to -1.27 (9,10-Difluorenone to 1,2-Benzenedicarboxylic acid). However, there were also transformation products with relatively high scores, such as B9 (9H-Fluorene-9-one, score: 1.57) and B10 (Benzophenone, score: 1.81), which warrant special attention in future studies.

To further investigate the toxicities of these transformation products, the lethal doses (LD50) and toxicity levels (**Fig. 6b** and **Table S7**) were predicted by the respiratory toxicity model in ProTox 3.0 (Banerjee et al. 2024). The findings indicated that as the transformation pathways progressed, the LD50 values of the products generally increased, except for 2,5-Cl₂Fluor, indicating a general toxicity decrement alongside XPAH transformation. For instance, the LD50 of 9,10-Cl₂Phe was 886 mg/kg with a toxicity level of 4. Among its transformation products, only B1 (Phe) had an LD50 (316 mg/kg, level 4) lower than that of 9,10-Cl₂Phe, while the toxicities of other oxidation and ring-opening products were lower. However, previous studies on the aryl hydrocarbon receptor activities of XPAHs in yeast assays reported the opposite results on toxicities of 9,10-Cl₂Phe and Phe: the relative equivalent potency of 9,10-Cl₂Phe was found to be much higher than Phe. In the case of 2,5-Cl₂Fluor, its inherently high LD50 (4220 mg/kg, level 5) resulted in most of its products having higher toxicity levels compared to the parent compound. Overall, most transformation products have toxicity levels lower than their precursors. However, given the disparities between model predictions and experimental results, further toxicity experiments are needed to substantiate the changes in toxicity during the transformation process of XPAHs.

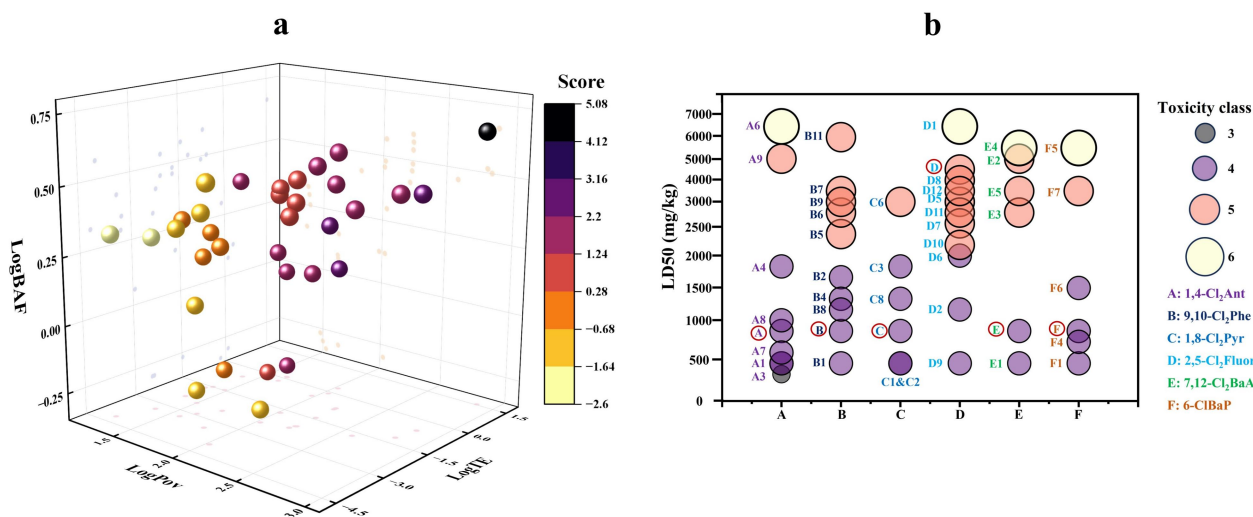


Fig. 6. (a) Prediction of environmental behaviors of XPAHs and their transformation products. (b) Respiratory toxicities (LD50) of XPAHs and their transformation products predicted by ProTox 3.0 model.

4. Conclusion

In summary, this study elucidated the mechanisms, influencing factors, pathways, and products involved in the conversion of XPAHs on PM through comprehensive field sampling and laboratory simulations. Experimental findings revealed that the molecular structures of PAHs exerted a significant influence on the conversion process, with dehalogenation and cleavage of the parent ring structure being prominent features of XPAHs conversion. The number and position of substituents further modulated the conversion dynamics. Key environmental parameters, including humidity, temperature, and H₂O₂ concentration, were identified as critical factors impacting conversion efficiency. The resulting conversion products and pathways were systematically hypothesized and confirmed, indicating a progressive decrease in environmental risks associated with the products as conversion advanced. This study provided novel insights into the heterogeneous conversion mechanisms of XPAHs on particulate matter, offering valuable contributions to the understanding of their environmental behavior and impact.

ASSOCIATED CONTENT

Author contributions

YY, RJ and MZ conceived the study and wrote the paper, YY, YL, GZ, SZ and XL performed the measurements and collected data. All authors contributed to the data analysis and review of the paper.

446 **Competing Interests**

447 The authors declare that they have no conflict of interest.

448 **Data availability**

449 All data are available from the authors upon request by contacting Rong Jin (jinrong@ucas.ac.cn).

450 **Supporting information**

451 Including detailed information on chemicals, sample testing and analysis data, screening of
452 chemical properties and toxicity prediction information, relevant parameters and data from simulation
453 experiments, as well as chromatograms for product identification.

454 **Acknowledgement**

455 The authors acknowledge the financial support provided by the Natural Science Foundation of Zhejiang
456 Province (Grant No. LQ22B070009), the National Natural Science Foundation of China (Grant No.
457 22106030), "Pioneer" and "Leading Goose" R&D Program of Zhejiang (Grant No. 2023C03157) and the
458 Research Funds of Hangzhou Institute for Advanced Study, UCAS (Grant No. 2023HIAS-Y014,
459 2022ZZ01017).

References

- Banerjee, P.; Kemmler, E.; Dunkel, M.; Preissner, R., 2024. ProTox 3.0: a webserver for the prediction of toxicity of chemicals. *Nucleic Acids Res* 10.1093/nar/gkae303
- Cao, Q.; Liu, Y.; Lyu, K.; Yu, Y.; Li, D.H.W.; Yang, L., 2020. Solar Radiation Zoning and Daily Global Radiation Models for Regions with Only Surface Meteorological Measurements in China. *Energ Convers Manage* 225, 10.1016/j.enconman.2020.113447
- Concha, C.; Manzano, C.A., 2023. Priority pesticides in Chile: Predicting their environmental distribution, bioaccumulation, and transport potential. *Integr Environ Assess Manag* 19, 676-683. 10.1002/ieam.4680
- Dang, J.; Shi, X.; Zhang, Q.; Hu, J.; Chen, J.; Wang, W., 2014. Mechanistic and Kinetic Studies on the OH-Initiated Atmospheric Oxidation of Fluoranthene. *Sci Total Environ* 490, 639-646. 10.1016/j.scitotenv.2014.04.134
- Deng, Q.X.; Feng, J.R.; Gao, P.P.; Ni, H.G., 2023. Combined effects of vehicles and waste incineration on urban air halogenated and parent polycyclic aromatic hydrocarbons. *Environ Int* 171, 107720. 10.1016/j.envint.2022.107720
- Hu, W.; Liu, D.; Su, S.; Ren, L.; Ren, H.; Wei, L.; Yue, S.; Xie, Q.; Zhang, Z.; Wang, Z.; Yang, N.; Wu, L.; Deng, J.; Qi, Y.; Fu, P., 2021. Photochemical Degradation of Organic Matter in the Atmosphere. *Adv Sustain Syst* 5, 10.1002/adsu.202100027
- Jia, H.; Zhao, S.; Shi, Y.; Zhu, K.; Gao, P.; Zhu, L., 2019. Mechanisms for Light-Driven Evolution of Environmentally Persistent Free Radicals and Photolytic Degradation of PAHs on Fe(III)-Montmorillonite Surface. *J Hazard Mater* 362, 92-98. 10.1016/j.jhazmat.2018.09.019
- Jin, R.; Liu, G.; Jiang, X.; Liang, Y.; Fiedler, H.; Yang, L.; Zhu, Q.; Xu, Y.; Gao, L.; Su, G.; Xiao, K.; Zheng, M., 2017a. Profiles, Sources and Potential Exposures of Parent, Chlorinated and Brominated Polycyclic Aromatic Hydrocarbons in Haze Associated Atmosphere. *Sci Total Environ* 593-594, 390-398. 10.1016/j.scitotenv.2017.03.134
- Jin, R.; Liu, G.; Zheng, M.; Jiang, X.; Zhao, Y.; Yang, L.; Wu, X.; Xu, Y., 2017b. Secondary Copper Smelters as Sources of Chlorinated and Brominated Polycyclic Aromatic Hydrocarbons. *Environ Sci Technol* 51, 7945-7953. 10.1021/acs.est.7b02031
- Jin, R.; Liu, G.; Zhou, X.; Zhang, Z.; Lin, B.; Liu, Y.; Qi, Z.; Zheng, M., 2023. Analysis of Polycyclic Aromatic Hydrocarbon Derivatives in Environment. *Trac-Trend anal chem* 160, 10.1016/j.trac.2023.116942
- Jin, R.; Yang, L.; Zheng, M.; Xu, Y.; Li, C.; Liu, G., 2018. Source identification and quantification of chlorinated and brominated polycyclic aromatic hydrocarbons from cement kilns co-processing solid wastes. *Environ Pollut* 242, 1346-1352. 10.1016/j.envpol.2018.08.025
- Jin, R.; Zheng, M.; Lammel, G.; Bandowe, B.A.M.; Liu, G., 2020. Chlorinated and Brominated Polycyclic Aromatic Hydrocarbons: Sources, Formation Mechanisms, and Occurrence in the Environment. *Prog Energy Combust Sci* 76, 10.1016/j.pecs.2019.100803
- Jin, R.; Zheng, M.; Yang, H.; Yang, L.; Wu, X.; Xu, Y.; Liu, G., 2017c. Gas-particle phase partitioning and particle size distribution of chlorinated and brominated polycyclic aromatic hydrocarbons in haze. *Environmental Pollution* 231, 1601-1608. 10.1016/j.envpol.2017.09.066
- Kakimoto, K.; Nagayoshi, H.; Konishi, Y.; Kajimura, K.; Ohura, T.; Hayakawa, K.; Toriba, A., 2014. Atmospheric chlorinated polycyclic aromatic hydrocarbons in East Asia. *Chemosphere* 111, 40-46. 10.1016/j.chemosphere.2014.03.072
- Kang, Q.; Bao, S.; Chen, B., 2021. Phototransformation of Three Polychlorinated Naphthalenes on

- Surface of Atmospheric Particulate Matter. *J Hazard Mater* 409, 124895. 10.1016/j.jhazmat.2020.124895
- Kitazawa, A.; Amagai, T.; Ohura, T., 2006. Temporal Trends and Relationships of Particulate Chlorinated Polycyclic Aromatic Hydrocarbons and Their Parent Compounds in Urban Air. *Environ Sci Technol* 40, 4592-4598.
- Lara, S.; Villanueva, F.; Martín, P.; Salgado, S.; Moreno, A.; Sánchez-Verdú, P., 2022. Investigation of PAHs, Nitrated PAHs and Oxygenated PAHs in PM10 Urban Aerosols. A Comprehensive Data Analysis. *Chemosphere* 294, 10.1016/j.chemosphere.2022.133745
- Laskin, A.; Laskin, J.; Nizkorodov, S.A., 2015. Chemistry of Atmospheric Brown Carbon. *Chem Rev* 115, 4335-4382. 10.1021/cr5006167
- Li, X.; Abdullah, L.C.; Sobri, S.; Md Said, M.S.; Hussain, S.A.; Aun, T.P.; Hu, J., 2023. Long-Term Air Pollution Characteristics and Multi-scale Meteorological Factor Variability Analysis of Megamountain Cities in the Chengdu-Chongqing Economic Circle. *Water Air Soil Pollut* 234, 328. 10.1007/s11270-023-06279-8
- Liu, Q.; Liggio, J.; Li, K.; Lee, P.; Li, S.M., 2019a. Understanding the Impact of Relative Humidity and Coexisting Soluble Iron on the OH-Initiated Heterogeneous Oxidation of Organophosphate Flame Retardants. *Environ Sci Technol* 53, 6794-6803. 10.1021/acs.est.9b01758
- Liu, Q.; Xu, X.; Wang, L.; Lin, L.; Wang, D., 2019b. Simultaneous Determination of Forty-Two Parent and Halogenated Polycyclic Aromatic Hydrocarbons Using Solid-Phase Extraction Combined with Gas Chromatography-Mass Spectrometry in Drinking Water. *Ecotoxicol Environ Saf* 181, 241-247. 10.1016/j.ecoenv.2019.06.011
- Ma, J.; Chen, Z.; Wu, M.; Feng, J.; Horii, Y.; Ohura, T.; Kannan, K., 2013. Airborne PM2.5/PM10-Associated Chlorinated Polycyclic Aromatic Hydrocarbons and Their Parent Compounds in a Suburban Area in Shanghai, China. *Environ Sci Technol* 47, 7615-7623. 10.1021/es400338h
- Malecha, K.; Nizkorodov, S., 2016. Photodegradation of Secondary Organic Aerosol Particles as a Source of Small, Oxygenated Volatile Organic Compounds. *Environ Sci Technol* 50, 9990-9997. 10.1021/acs.est.6b02313
- Nilsson, U.L.; Ostman, C.E., 1993. CHLORINATED POLYCYCLIC AROMATIC-HYDROCARBONS - METHOD OF ANALYSIS AND THEIR OCCURRENCE IN URBAN AIR. *Environmental Science & Technology* 27, 1826-1831. 10.1021/es00046a010
- Nishimura, C.; Horii, Y.; Tanaka, S.; Asante, K.A.; Ballesteros, F., Jr.; Viet, P.H.; Itai, T.; Takigami, H.; Tanabe, S.; Fujimori, T., 2017. Occurrence, Profiles, and Toxic Equivalents of Chlorinated and Brominated Polycyclic Aromatic Hydrocarbons in E-Waste Open Burning Soils. *Environ Pollut* 225, 252-260. 10.1016/j.envpol.2016.10.088
- Noro, K.; Omagari, R.; Ito, K.; Wang, Q.; Sei, K.; Miyake, Y.; Amagai, T., 2023. Sampling, Pretreatment, Instrumental Analysis, and Observed Concentrations of Polycyclic Aromatic Hydrocarbons, Polychlorinated Naphthalenes, and Halogenated Polycyclic Aromatic Hydrocarbons: A Review. *Trac-Trend anal chem* 169, 10.1016/j.trac.2023.117384
- Ohura, T.; Amagai, T.; Makino, M., 2008. Behavior and Prediction of Photochemical Degradation of Chlorinated Polycyclic Aromatic Hydrocarbons in Cyclohexane. *Chemosphere* 70, 2110-2117. 10.1016/j.chemosphere.2007.08.064
- Ohura, T.; Horii, Y.; Kojima, M.; Kamiya, Y., 2013. Diurnal Variability of Chlorinated Polycyclic Aromatic Hydrocarbons in Urban Air, Japan. *Atmos Environ* 81, 84-91. 10.1016/j.atmosenv.2013.08.044
- Ohura, T.; Morita, M.; Makino, M.; Amagai, T.; Shimoi, K., 2007. Aryl Hydrocarbon Receptor-Mediated

- Effects of Chlorinated Polycyclic Aromatic Hydrocarbons. *Chem Res Toxicol* 20, 1237–1241.
- Ohura, T.; Sakakibara, H.; Watanabe, I.; Shim, W.J.; Manage, P.M.; Guruge, K.S., 2015. Spatial and vertical distributions of sedimentary halogenated polycyclic aromatic hydrocarbons in moderately polluted areas of Asia. *Environ Pollut* 196, 331-340. 10.1016/j.envpol.2014.10.028
- Ohura, T.; Savada, K.; Amagai, T.; Shinomiya, M., 2009. Discovery of Novel Halogenated Polycyclic Aromatic Hydrocarbons in Urban Particulate Matters: Occurrence, Photostability, and AhR Activity. *Environ Sci Technol* 43, 2269–2275.
- Sei, K.; Wang, Q.; Tokumura, M.; Miyake, Y.; Amagai, T., 2021. Accurate and Ultrasensitive Determination of 72 Parent and Halogenated Polycyclic Aromatic Hydrocarbons in a Variety of Environmental Samples via Gas Chromatography-Triple Quadrupole Mass Spectrometry. *Chemosphere* 271, 129535. 10.1016/j.chemosphere.2021.129535
- Shannon, R.D., 1976. Revised effective ionic radii and systematic studies of interatomic distances in halides and chalcogenides. *Acta Crystallographica Section A* 32, 751-767. 10.1107/s0567739476001551
- Shiraishi, H.; Pilkington, N.H.; Otsuki, A.; Fuwa, K., 1985. Occurrence of chlorinated polynuclear aromatic hydrocarbons in tap water. *Environ Sci Technol* 19, 585-590. 10.1021/es00137a001
- Shiraiwa, M.; Ammann, M.; Koop, T.; Pöschl, U., 2011. Gas uptake and chemical aging of semisolid organic aerosol particles. *Proc Natl Acad Sci USA* 108, 11003-11008. 10.1073/pnas.1103045108
- Sun, J.L.; Zeng, H.; Ni, H.G., 2013. Halogenated polycyclic aromatic hydrocarbons in the environment. *Chemosphere* 90, 1751-1759. 10.1016/j.chemosphere.2012.10.094
- Takikawa, T.; Wang, Q.; Omagari, R.; Noro, K.; Miyake, Y.; Amagai, T., 2023. Development of an Analytical Method for Indoor Polycyclic Aromatic Hydrocarbons and Their Halogenated Derivatives by Using Thermal Separation Probe Coupled to Gas Chromatography-Tandem Mass Spectrometry. *Sci Total Environ* 903, 166931. 10.1016/j.scitotenv.2023.166931
- Vuong, Q.T.; Thang, P.Q.; Nguyen, T.N.T.; Ohura, T.; Choi, S.-D., 2020. Seasonal variation and gas/particle partitioning of atmospheric halogenated polycyclic aromatic hydrocarbons and the effects of meteorological conditions in Ulsan, South Korea. *Environmental Pollution* 263, 10.1016/j.envpol.2020.114592
- Wang, T.; Liu, Y.; Deng, Y.; Cheng, H.; Yang, Y.; Feng, Y.; Zhang, L.; Fu, H.; Chen, J., 2020. Photochemical Oxidation of Water-Soluble Organic Carbon (WSOC) on Mineral Dust and Enhanced Organic Ammonium Formation. *Environ Sci Technol* 54, 15631-15642. 10.1021/acs.est.0c04616
- Wang, Y.; Su, P.; Ge, X.; Ren, H.; Ma, S.; Shen, G.; Chen, Q.; Yu, Y.; An, T., 2022. Identification of specific halogenated polycyclic aromatic hydrocarbons in surface soils of petrochemical, flame retardant, and electronic waste dismantling industrial parks. *J Hazard Mater* 436, 129160. 10.1016/j.jhazmat.2022.129160
- Xia, Z.; Idowu, I.; Marvin, C.; Thomas, P.J.; Johnson, W.; Francisco, O.; Stetefeld, J.; Crimmins, B.; Fry, M.; Tomy, G.T., 2019. Identification of halogenated polycyclic aromatic hydrocarbons in biological samples from Alberta Oil-Sands Region. *Chemosphere* 215, 206-213. 10.1016/j.chemosphere.2018.10.050
- Xie, J.; Tao, L.; Wu, Q.; Lei, S.; Lin, T., 2021. Environmental Profile, Distributions and Potential Sources of Halogenated Polycyclic Aromatic Hydrocarbons. *J Hazard Mater* 419, 10.1016/j.jhazmat.2021.126164
- Yang, L.; Shen, J.; Zheng, M.; Yang, Q.; Li, D.; Liu, G., 2022a. Occurrence of chlorinated and brominated polycyclic aromatic hydrocarbons from electric arc furnace for steelmaking. *Environ*

Pollut 294, 118663. 10.1016/j.envpol.2021.118663

Yang, Y.; Liu, G.; Zheng, M.; Liu, S.; Yang, Q.; Liu, X.; Wang, M.; Yang, L., 2022b. Discovery of significant atmospheric emission of halogenated polycyclic aromatic hydrocarbons from secondary zinc smelting. *Ecotoxicol Environ Saf* 238, 113594. 10.1016/j.ecoenv.2022.113594

Zhang, L.; Yan, W.; Kohtani, S.; Fukuyoshi, S.; Hu, M.; Nagao, S.; Tang, N., 2024. Promotive Effects of Marine-Derived Dimethyl Sulfoxide on the Photodegradation of Phenanthrene in the Atmosphere. *Sci Total Environ* 926, 171938. 10.1016/j.scitotenv.2024.171938

Zhang, L.H.; Li, P.J.; Gong, Z.Q.; Oni, A.A., 2006. Photochemical behavior of benzo[a]pyrene on soil surfaces under UV light irradiation. *J Environ Sci (China)* 18, 1226-1232. 10.1016/s1001-0742(06)60067-3

Zhang, Q.; Wang, Y.; Gao, M.; Li, Y.; Zhao, L.; Yao, Y.; Chen, H.; Wang, L.; Sun, H., 2023. Organophosphite Antioxidants and Novel Organophosphate Esters in Dust from China: Large-Scale Distribution and Heterogeneous Phototransformation. *Environ Sci Technol* 57, 4187-4198. 10.1021/acs.est.2c08239

Zhao, S.; Jia, H.; Nulaji, G.; Gao, H.; Wang, F.; Wang, C., 2017. Photolysis of Polycyclic Aromatic Hydrocarbons (PAHs) on Fe(³⁺)-Montmorillonite Surface Under Visible Light: Degradation Kinetics, Mechanism, and Toxicity Assessments. *Chemosphere* 184, 1346-1354. 10.1016/j.chemosphere.2017.06.106

Zhu, J.; Sheng, M.; Shang, J.; Kuang, Y.; Shi, X.; Qiu, X., 2022. Photocatalytic Role of Atmospheric Soot Particles under Visible-Light Irradiation: Reactive Oxygen Species Generation, Self-Oxidation Process, and Induced Higher Oxidative Potential and Cytotoxicity. *Environ Sci Technol* 56, 7668-7678. 10.1021/acs.est.2c00420